



HAL
open science

Synchronized observations of bright points from the solar photosphere to the corona

Ehsan Tavabi

► **To cite this version:**

Ehsan Tavabi. Synchronized observations of bright points from the solar photosphere to the corona. Monthly Notices of the Royal Astronomical Society, 2018, 476 (1), pp.868 - 874. 10.1093/mnras/sty020 . hal-01774849

HAL Id: hal-01774849

<https://hal.sorbonne-universite.fr/hal-01774849v1>

Submitted on 24 Apr 2018

HAL is a multi-disciplinary open access archive for the deposit and dissemination of scientific research documents, whether they are published or not. The documents may come from teaching and research institutions in France or abroad, or from public or private research centers.

L'archive ouverte pluridisciplinaire **HAL**, est destinée au dépôt et à la diffusion de documents scientifiques de niveau recherche, publiés ou non, émanant des établissements d'enseignement et de recherche français ou étrangers, des laboratoires publics ou privés.



Distributed under a Creative Commons Attribution 4.0 International License

Synchronized observations of bright points from the solar photosphere to the corona

Ehsan Tavabi^{1,2,3}★

¹Physics Department, Payame Noor University (PNU), 19395-3697 Tehran, Iran

²Research Institute for Applied Physics and Astronomy (RIAPA), University of Tabriz, Tabriz 51665-163, Iran

³Institut d'Astrophysique de Paris, UMR 7095, CNRS and UPMC, 98 Bis Bd Arago, F-75014 Paris, France

Accepted 2018 January 3. Received 2017 December 30; in original form 2017 October 17

ABSTRACT

One of the most important features in the solar atmosphere is the magnetic network and its relationship to the transition region (TR) and coronal brightness. It is important to understand how energy is transported into the corona and how it travels along the magnetic field lines between the deep photosphere and chromosphere through the TR and corona. An excellent proxy for transportation is the *Interface Region Imaging Spectrograph* (*IRIS*) raster scans and imaging observations in near-ultraviolet (NUV) and far-ultraviolet (FUV) emission channels, which have high time, spectral and spatial resolutions. In this study, we focus on the quiet Sun as observed with *IRIS*. The data with a high signal-to-noise ratio in the Si IV, C II and Mg II k lines and with strong emission intensities show a high correlation with TR bright network points. The results of the *IRIS* intensity maps and dopplergrams are compared with those of the Atmospheric Imaging Assembly (AIA) and Helioseismic and Magnetic Imager (HMI) instruments onboard the *Solar Dynamical Observatory* (*SDO*). The average network intensity profiles show a strong correlation with AIA coronal channels. Furthermore, we applied simultaneous observations of the magnetic network from HMI and found a strong relationship between the network bright points in all levels of the solar atmosphere. These features in the network elements exhibited regions of high Doppler velocity and strong magnetic signatures. Plenty of corona bright points emission, accompanied by the magnetic origins in the photosphere, suggest that magnetic field concentrations in the network rosettes could help to couple the inner and outer solar atmosphere.

Key words: Sun: corona – Sun: magnetic fields – Sun: transition region.

1 INTRODUCTION

The quiet Sun observed in the chromospheric layers is dominated by magnetic bright points (MBPs), or the magnetic network at rosettes of supergranule cells (Dunn & Zirker 1973; Tavabi 2014). These chromospheric bright points do not, however, definitely correspond to the photospheric bright-point elements (Muller et al. 2000). Simon & Leighton (1964) found a strong correlation between the chromospheric network magnetic map and quiet Sun supergranulation processes using spectroheliograms, dopplergrams and magnetograms, but the interaction between the magnetic field in the network (~ 1 kG) and the dynamical flow at the boundary of these giant cells has not been theoretically established, and several incompatibilities between supergranulation and the magnetic network have been reported (Snodgrass & Ulrich 1990). Today, this relationship is generally accepted, suggesting that the formation of

the magnetic network is strongly associated with supergranulation flows (Roudier et al. 2009).

A supergranule rosette normally represents several obvious MBPs with high magnetic field strength, while the internetwork bright points are associated with much weaker magnetic fields (Zirin 1993; Keller 1992). The morphology and migration of MBPs can be described as random wandering caused by the convection turbulence resulting from supergranular flows from the centre to the edge of the cell (Lawrence & Schrijver 1993; Jafarzadeh et al. 2014).

The coronal cells are centred on the enhanced network elements of large-scale regions, and no evidence has been found for their relationship to internetwork regions. Hagenaar et al. (1997) investigated the cellular patterns of the supergranular network, and their model shows that the range in outflow strengths is remarkably small in the higher chromosphere.

Using the cross-correlation method between a magnetogram and dopplergram, Wang & Zirin (1989) confirmed that the supergranule boundaries and magnetic network are roughly correlated and they obtained good observational support for the relationship between

* E-mail: tavabi@iap.fr

the supergranular magnetic structures and line-of-sight velocities. Coronal bright points (CBPs) have been seen with the help of X-ray and extreme ultraviolet (EUV) telescopes (Golub et al. 1974; Habbal & Withbroe 1981). At large scales, the distribution of CBPs over the solar surface is uniform (Golub et al. 1975), with some deviations from uniformity at latitudes typical for active regions. Golub et al. (1977) found that all X-ray CBPs appear in magnetograms as bipolar features, and the separation distance of the bipoles increases with their age. The velocity of the separating motion is of the order of 2 km s^{-1} , and the typical total magnetic flux ranges from 10^{19} to 10^{20} Mx per day of lifetime. The convergence of the bipoles and full cancellation of magnetic elements of opposite polarity have already been reported (e.g. see Madjarska et al. 2003).

Kayshap & Dwivedi (2017) found that some of the CBPs are formed through the convergence of bipolar magnetic fields, while others appear through the emergence of a new magnetic field. Koutchmy et al. (1997) provided evidence of soft X-ray brightening events known as coronal flashes. These features have a short lifetime and could be associated with X-ray jets. Sheeley & Golub (1979) found that a CBP consists of several miniature loops (each ~ 25 Mm in diameter and 12 Mm long), and Alipour & Safari (2015) found two main categories of lifetime for CBPs: 52 per cent show short lifetimes typically of less than 20 min, and the remaining 48 per cent show long lifetimes of 6 hr. It seems to be necessary to identify and track the anchors of the CBPs in order to understand their sources and physical properties.

A large number of the HMI magnetic bright points, which are dominated by small-scale bright dots, tend to recur at roughly the same location in the photosphere. These characteristics, associated in TR dopplergrams with areas of high line-of-sight velocities, suggest that some of these bright points may result from magnetic reconnections of loops (Tavabi et al. 2015) at source regions in the lower layers of the TR and chromosphere. Because the position of the coronal magnetic field makes direct measurements almost impossible, the magnetic structure and its properties can be understood only indirectly, through the characteristics of the surrounding magnetic structure.

Filippov et al. (2009) determined the geometrical shape of the jets, which show a frozen vertical ejection of hot plasma into the higher atmosphere that could introduce rapid heating of the corona and a mass source into the solar wind flow. It may be expected that these CBPs could also be traced throughout the TR and chromosphere, given that the photospheric magnetic field lines continually expand towards the corona.

Dopplergrams are the oldest technique used to find supergranulation. The first detection was made by Hart (1954), and the typical length of these structures ranges between about 20 and 30 Mm (Simon & Leighton 1964). We investigate the relationship between the photospheric magnetic field, chromospheric, and TR dopplergrams in near-ultraviolet (NUV) and far-ultraviolet (FUV) emission channels with coronal EUV filtergrams.

2 OBSERVATIONS

AIA/*SDO* is an array of four telescopes capturing images of the Sun's atmosphere out to $1.3R_{\odot}$ in 10 separate EUV wavebands (Title et al. 2006). The images are 4096×4096 pixel², with a pixel size of 0.6 arcsec in full spatial resolution mode and a cadence of 12 s on 2014 July 2 (Fig. 1). HMI/*SDO* observes the full disc in the Fe I absorption line at 6173 Å with a pixel size of ~ 0.5 arcsec, using mechanical shutters and control electronics to take a 45-s line-of-sight magnetic field sequence (Pesnell et al. 2012).

AIA observes simultaneously in the best signal-to-noise ratio channels at 304 Å (He II, chromosphere and TR, 50 kK), 171 Å (Fe IX, TR and corona, 6300 kK), and 193 Å (Fe XII, XXIV, corona and flares, 1.2 MK). *IRIS* observations with a spatial resolution of 0.3–0.4 arcsec, a pixel size of 0.166 arcsec (corresponding to 120 km at the disc centre) and high cadence reveal the dynamical behaviour of the chromosphere and of TR fine features (De Pontieu et al. 2014). The high cadence allows the evolution of these features to be analysed and enables us to follow them from the photosphere to the low corona in three channels of different spectral lines, namely in the near-ultraviolet (NUV) (2782–2835 Å with the Mg II H and k resonance lines seen in the absorption on-disc and in emission off-disc, similar to the well-known H and K lines of Ca II), in the far-ultraviolet (FUV) (1331–1358 Å with the C II line seen in emission), and in 1389–1407 Å (with the Si IV lines seen in emission).

Note that the Mg II lines belong to a low-first ionization potential (FIP) element typical for a low-temperature plasma situated above the temperature minimum near heights of about 500 km, above $\tau_{500} = 1$. The FIP of Mg is 7.65 eV. The Ca II line is emitted by a high-FIP element with excitation potential corresponding to a higher temperature. The Si IV lines are produced at much higher temperatures, with an ionization potential of Si^{IV} of 33.5 eV.

The velocity resolution in *IRIS* spectra is 0.5 km s^{-1} . In addition, slit-jaw images (SJIs) with a 166×175 arcsec² field-of-view (FOV) that reflect off the slit/prism assembly through a filter wheel with four different filters (De Pontieu et al. 2014) are available. This region is located at the centre of the solar disc (Fig. 1), where it is quiet, and no active region is observed. It is not a coronal hole region. Some patches of concentrated magnetic field can, however, exist in the FOV. Fig. 1 provides a synoptic image of the region seen in 171-Å Fe IX emission from the AIA (*SDO* mission) observations during the *IRIS* observations as reported here.

A very large dense *IRIS* raster over the Sun's disc centre was performed on 2014 July 2 at 12:12 to 14:00 UT with a cadence of 16.3 s centred at $[49.^{\circ}4; -4.^{\circ}3]$. The raster covered about 141×175 arcsec² and took about 2 h to complete. Calibrated level 2 data were used; the raster cadence is of the order of 16 s, with a spatial step of 0.35 arcsec; the 400-pixel long slit covers 141×175 arcsec². The SJ high-resolution images were obtained in two channels, showing (i) the low temperature of the TR in C II (1335 Å, $\log T \sim 3.6$ to 4), and (ii) the much hotter TR in Si IV (lines near 1400 Å with $\log T \sim 4.8$); their maximum FOV is also 306×175 arcsec² (Fig. 4), with a 32-s cadence and pixel size of the order of 0.1 arcsec, including 199 SJ frames for each filter (Tavabi et al. 2015).

3 RESULTS

From Figs 2 to 6, it is clear that the supergranular cell velocity map is concentrated at the network, and much larger line-of-sight velocities and population density occurs at the rosettes, as the signal almost disappears near the centre of cells, which is defined as inter-network regions and the flows are dominated by horizontal motions. The bright point intensity fluctuations are considered using the SJIs (1400 and 1335 Å) and constructed dopplergrams (Fig. 2) from the dense raster containing spectral information in the NUV (Mg II K, 2796 Å) resonance line and FUV (C II and Si IV in 1335- and 1400-Å) *IRIS* observations, and AIA and HMI on the *SDO* mission in different channel time series. The velocity resolution of the dopplergrams is about $\pm 0.5 \text{ km s}^{-1}$. The dopplergrams are constructed by subtracting red- and blue-wing intensities of spectral lines at fixed offset velocities from the centre of the line, for example $\pm 50 \text{ km s}^{-1}$.

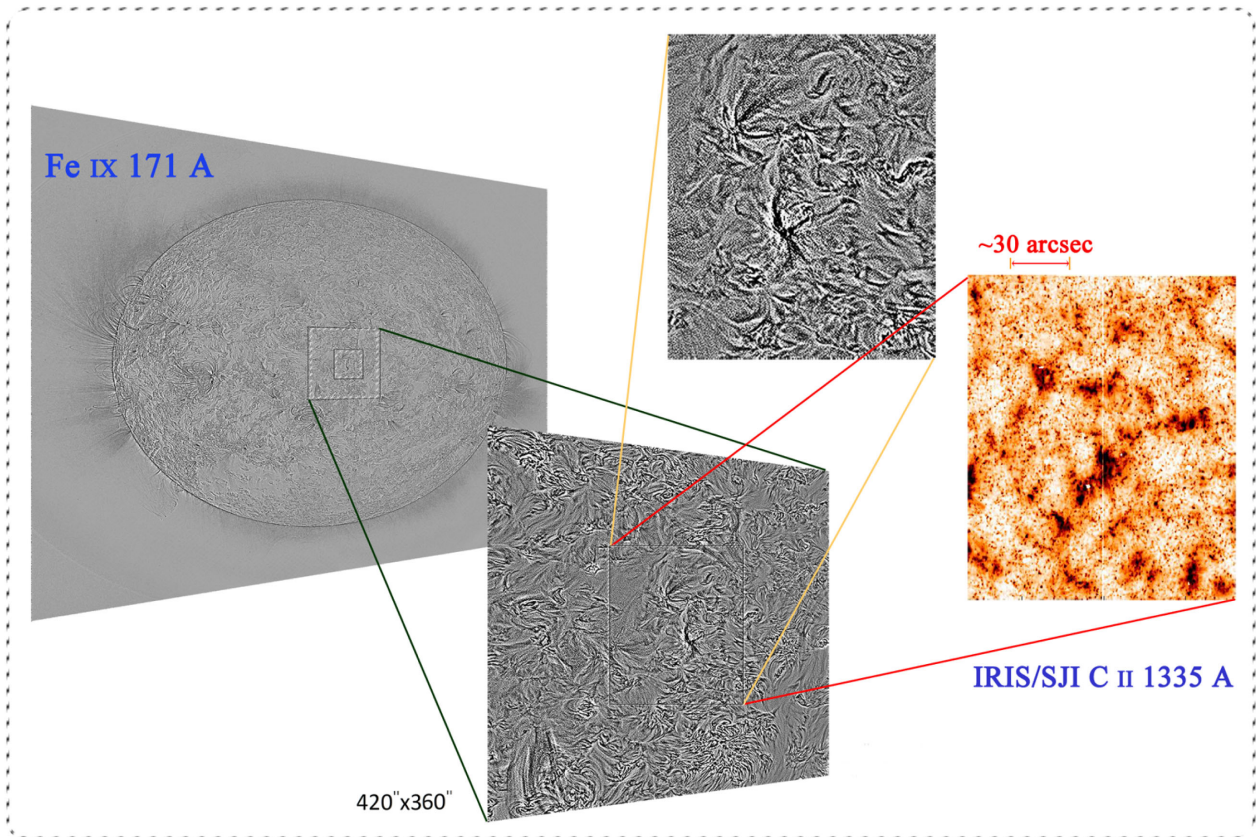


Figure 1. The full disc observation of AIA/SDO in the Fe IX 171-Å line after summing over 30 min with a 12-s cadence on 2014 June 2 beginning at 12:12 UT (left panel). The region was observed simultaneously by IRIS (right panel) in several transition region layers.

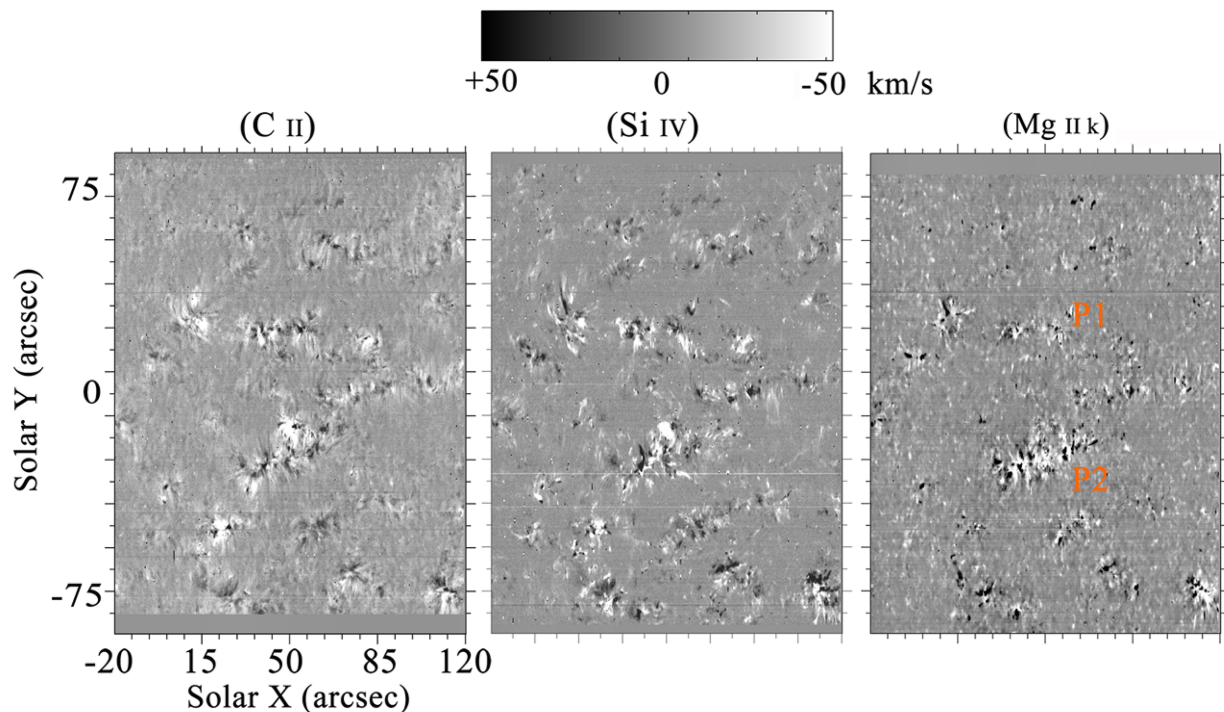


Figure 2. Filtered in the velocity space (white is for blueshifts and black for redshifts). The first panel is for C II (1335 Å), the second is for Si IV (1393 Å), and the third is for Mg II κ (2796 Å). The two positions with high values of downward velocity are marked by P1 and P2 (Fig. 3). The vertical and horizontal axes indicate the distance in arcseconds. The spatial resolutions of raster dopplergrams are adequate, in most cases, to resolve the details of the dynamical aspect of the magnetic bright points.

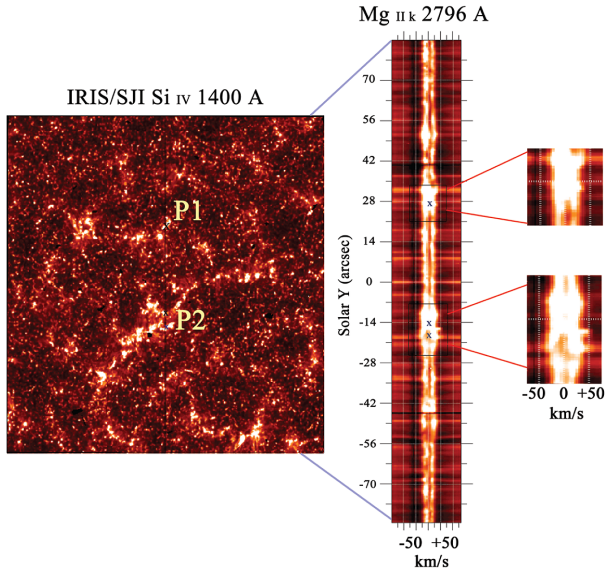


Figure 3. Spatial-temporal properties of bright points. Rapidly evolving bright points are short-lived with bright features in the blue and red wings (e.g. around $\pm 50 \text{ km s}^{-1}$) of the chromospheric $\text{Mg II } \kappa$ 2796-Å spectral line and $\text{Si IV } 1403$ -Å slit-jaw image. Highly contrasted and magnified simultaneous spectrograms of the slit position in the $\text{Mg II } \kappa$ line taken on 2014 June 2 at 13:13:01 UT. The direction perpendicular to the image plane is evident in this line by the large Doppler effects at positions shown by marks (scale on the left).

Fig. 3 shows an SJI with faint roundish bright points in the hot FUV filtergrams (1400 Å, $T \sim 80 \text{ kK}$), near the centre of the FOV, with the entrance slit of the spectrograms crossing the region at 13:13 UT. These points are marked by P1, and double points at P2, and are clearly seen as evidence examples in simultaneous NUV cool spectral channel. ($\text{Mg II } \kappa$, 2796 Å, $T \sim 10 \text{ kK}$) in the right panel. This region is almost at the centre of the solar disc.

Fig. 4 shows integrated intensity maps for SJIs in both *IRIS* filtergrams, and the region between the dotted vertical lines corresponds to the FOV of Fig. 2 velocity map. To emphasize the bright points with higher visibility and decrease the effect of smaller and short-lifetime brightening, we only observed the prominent region directly related to the TR network. This series was chosen because it is congruent with our primary aim to study MBPs precisely and to evaluate a plausible trajectory with height with respect to photosphere magnetograms, chromospheres and TR dopplergrams (Figs 2 to 4). Sheeley & Warren (2012) found this type of cellular feature in $\text{Fe XII } 193$ -Å filtergrams of the 1.2-MK corona. It is also confirmed with the *IRIS* dopplergram in the Si IV line (Figs 2, 5 and 6 middle panels) that there are mostly downflows in the network, which look reddish in the Doppler map.

Here, the *IRIS*-wavelength dopplergrams demonstrate highly correlated dynamical behaviours, and upward (and downward) motions are observed mainly at the boundaries of supergranular cells (Figs 3 and 4). The correlation coefficient for the dopplergrams in different lines in network regions increases to more than 90 per cent (Fig. 5).

Fig. 6 reveals that most of the high-velocity elements coincide with the magnetic network concentrations. The network elements are also close to bright points in the *IRIS* SJ images (Figs 3, 4 and 5). Fig. 7 illustrates the positions of TR bright points in Si IV (+ marks) and C II (* marks) in the solar quiet region in the same FOV AIA/*SDO* observation channels as the background snapshots. The physical properties and formation temperature of these two

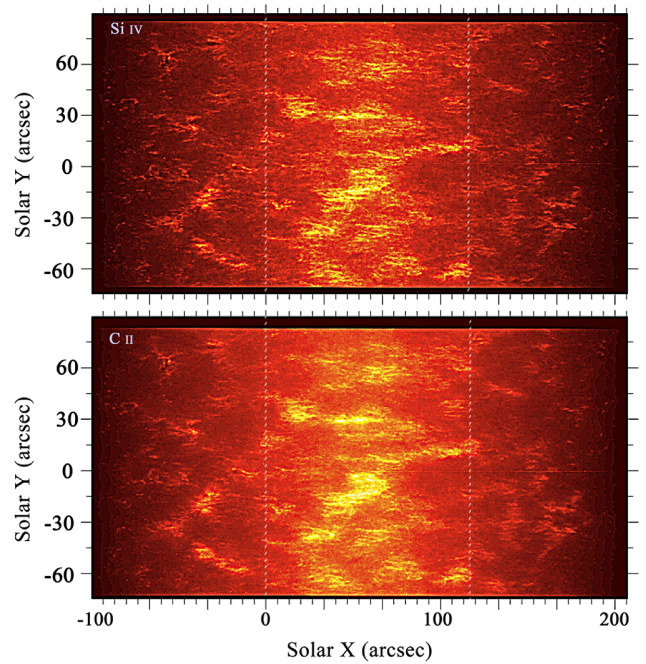


Figure 4. Time-integrated slit-jaw image (SJI) maps of the maximum field of view (FOV), $\text{Si IV } 1400$ Å (top) and $\text{C II } 1335$ Å (bottom), illustrate the moving SJIs (from left to right) for the full interval of observation on 2014 July 2 from 12:12 to 14:00 UT with a cadence of 16.3 s centred at $[49.''4; -4.''3]$. The SJI maps covered about $(\sim 306 \times 175 \text{ arcsec}^2)$ and took about 2 h to complete. The vertically dotted lines show the FOV of the dopplergrams ($141 \times 175 \text{ arcsec}^2$).

IRIS lines closely resemble one another, so these brightenings seem to show the same layer. The shape and size of bright points in both lines are the same, with small differences in number. They appear and disappear almost simultaneously (Tavabi et al. 2015; Martinez-Sykora et al. 2015). We integrated the moving SJIs from the beginning to the end of the observation series to obtain a maximum FOV ($\sim 306 \text{ arcsec} \times 175 \text{ arcsec}$).

Fig. 4 presents such time-integrated intensity maps of SJIs, and in Fig. 7 all brightenings of SJIs are compared with the corresponding synthetic AIA filtergrams. AIA images, including the 150 frames in each wavelength channel, have also been integrated over 30 min to increase the signal-to-noise ratio. A close examination of the intensity map reveals the faint presence of small differences at internetwork bright points, while they are in high compliance with the network. By comparing the *IRIS* and AIA filtergrams, we found correlated coronal brightenings for all prominent TR bright points in network regions, which could be interpreted as a consequence of field-aligned plasma motion and give an indirect diagnosis of the trajectory of frozen-in magnetic plasma flows between the TR and the corona through the layers.

In order to do this, we considered the intensity fluctuation diagrams in detail for the TR network brightening associated with coronal patches of bright points (Fig. 8). These samples are marked with numbers and show four rather isolated magnetic bright points in the network. These points are observed in both *IRIS* SJIs and time-integrated AIA filtergrams over 30 min that correspond to this region simultaneously (see Fig. 8).

Almost all coronal bright points can clearly be discerned in space at different wavelengths. The bright points in the 1335- and 1400-Å emission lines seem to come from the same layer, and show an exactly coherent behaviour in intensity variations with a good time

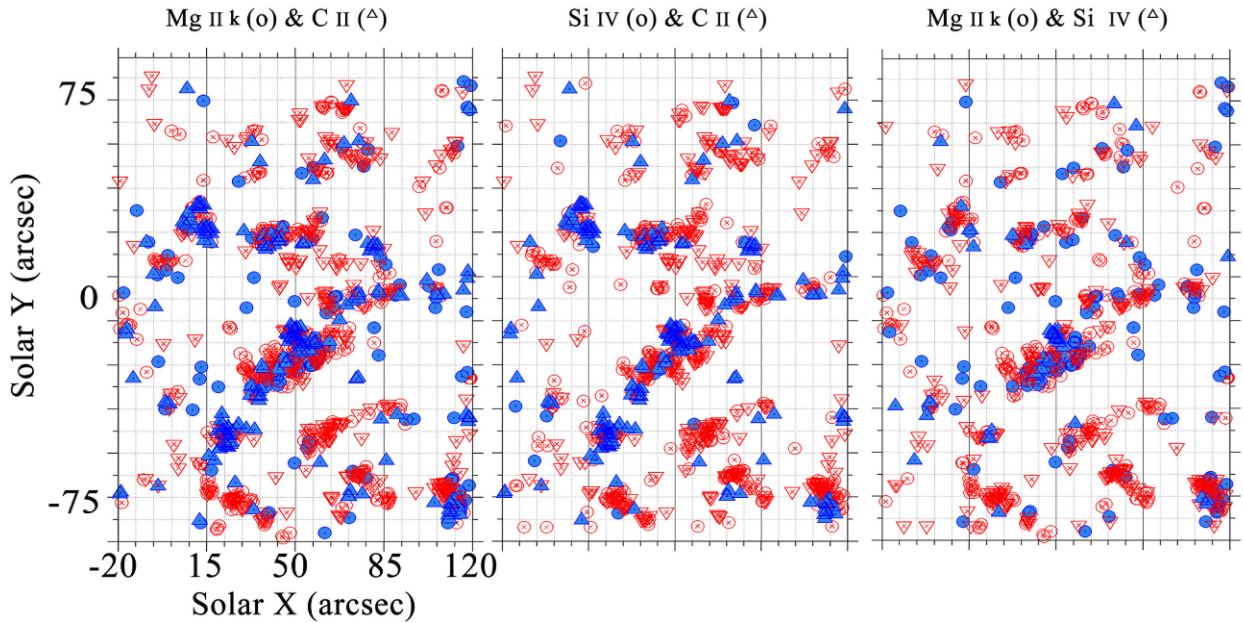


Figure 5. Distribution of high-velocity elements in the studied region for three *IRIS* lines. Red (blue) symbols with crosses (dots) inside show downward (upward) motions. The correlation coefficient between pairs of distributions reaches >90 per cent for different *IRIS* lines.

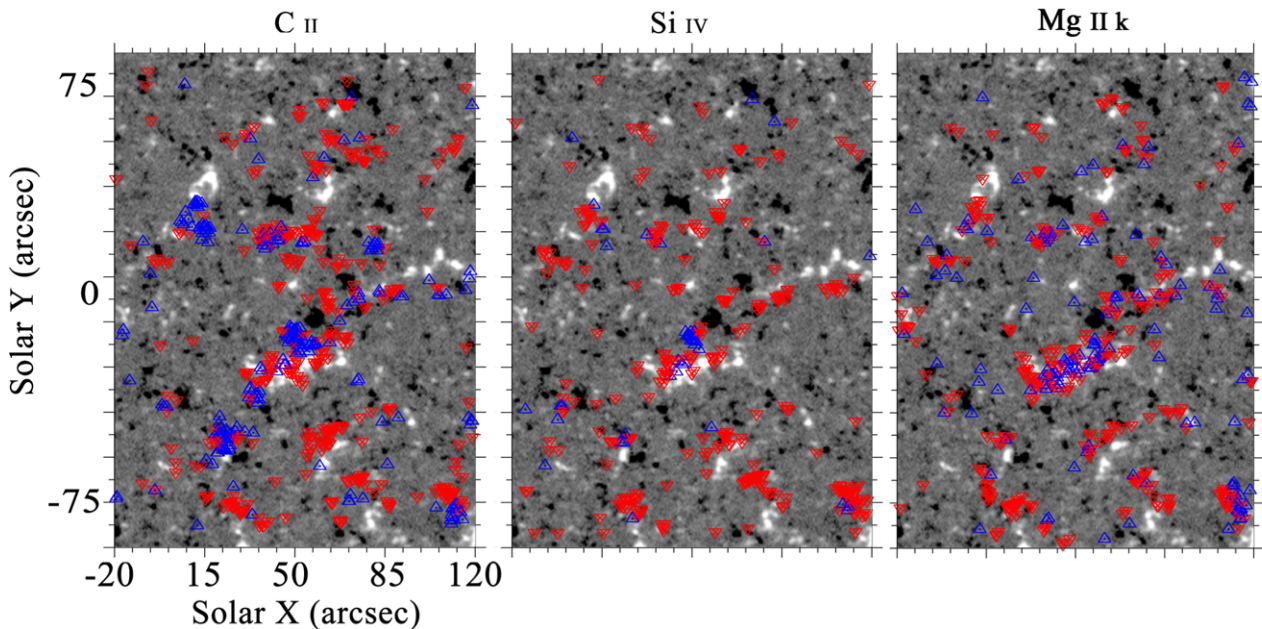


Figure 6. Comparative diagrams show dopplergram high-velocity positions on the HMI/SDO magnetograms for this region for three lines.

match (Martinez-Sykora et al. 2015). These marked points as a collection of smaller bright points are associated with cluster counterparts in coronal patches with enhanced emission.

In order to inspect their dynamical behaviours and intensity profiles in detail, we chose these points, as they could be well placed in the TR network and are easy to distinguish from the background intensity. These points exist in all lines in the TR with a strong intensity variation on short time-scales that is higher than the temporal resolution of the observation cadences.

The variations exhibit a pseudo-oscillatory behaviour without a constant frequency in different cases and a regular period of time

(Figs 9 and 10). Therefore, the data seem to suggest that the coronal portion of bright points is heated by some mechanism and then it cools down by radiation and thermal conduction to the TR temperature, when it is then heated (Habbal & Withbroe 1981).

The correspondence of temporal variations between the coronal and *IRIS* data of the TR in these bright points is expected to be better for 171- and 304-Å line filtergrams, because the temperatures are closer. Thus, a better time correlation between the corresponding intensity changes is seen in the middle and bottom panels of Figs 9 and 10. Here, it should be emphasized that the intensity variations are caused by an increase in the intensity of the individual pixels

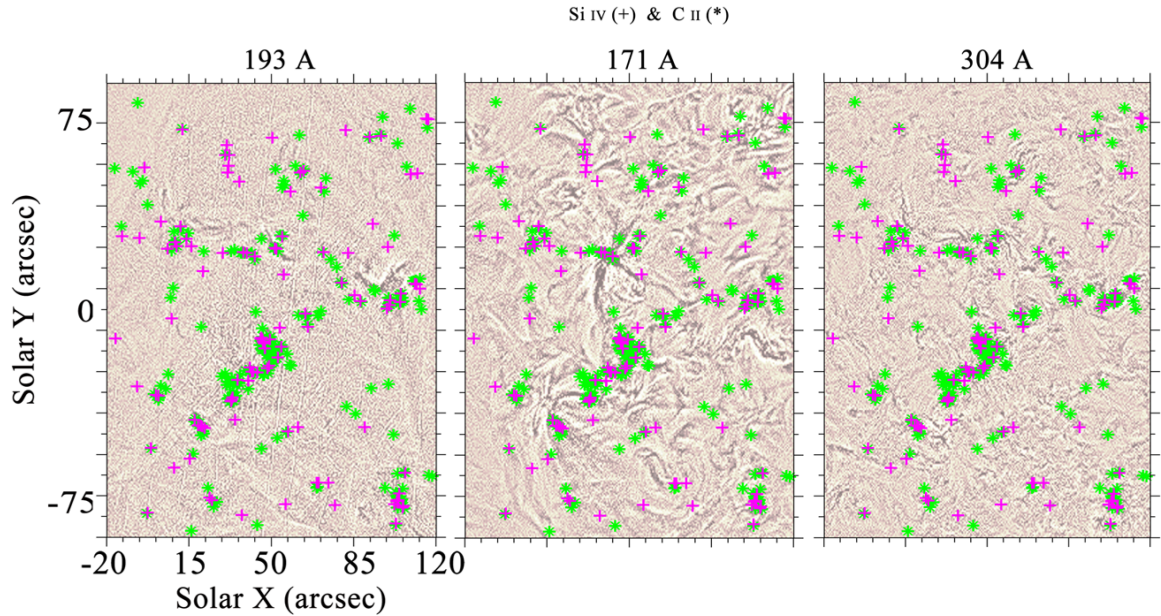


Figure 7. The bright points in transition-region slit-jaw images from *IRIS* and AIA/*SDO* hot lines show a significant 2D correlation. The background images are the sum results of frames in 30 min. After applying the ‘unsharpmask’ filter to the 193-Å images, we see long straight lines displaying the readout pixels of the AIA CCD camera.

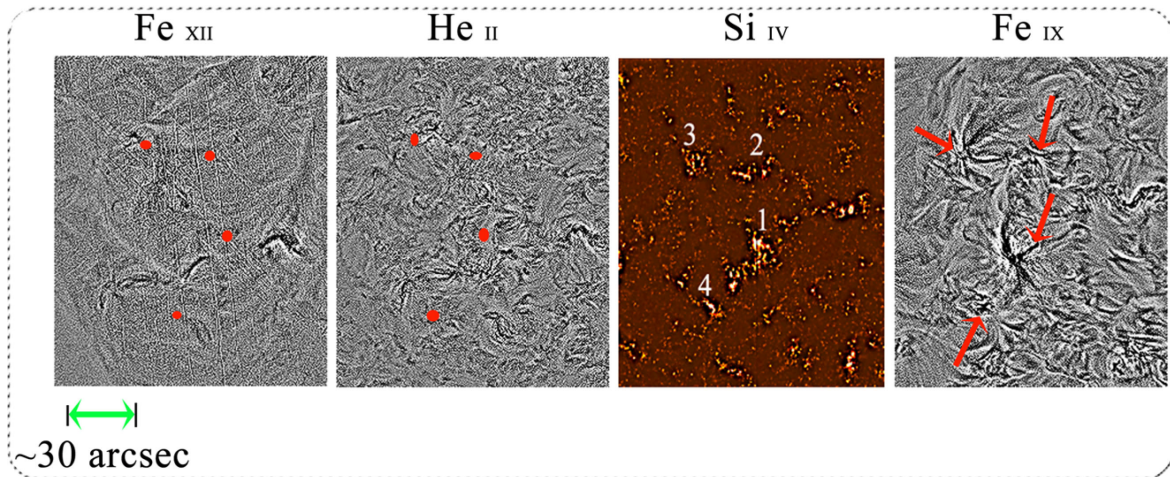


Figure 8. Regions extracted from Fig. 1, displaying the same field of view as *IRIS* observations. Some prominent magnetic bright points marked by numbers in the Si iv slit-jaw image are marked by arrows in other panels.

after integrating over the area that covers the bright point site. This is not related to a change in their numerical population. Almost all of these bright points show the same type of variations in the intensity accompanied with the associated regions in the TR layer, variations in the intensity accompanied with the associated regions in the TR layer, which have been plotted synchronously with the *SJI/IRIS* profiles for the same positions.

4 CONCLUSIONS

In this study, we used co-observations from HMI, AIA and *IRIS* instruments that contain photospheric magnetic field, TR and coronal data, including NUV and FUV spectra of the chromosphere, TR, and coronal filtergrams from the AIA to establish an indirect correlation between bright features observed in the quiet Sun.

HMI magnetograms indicate that field lines are strongly concentrated at photosphere footpoints. Furthermore, it is likely that the field lines expand into the corona. Our comparative analyses revealed a strong connection between coronal bright patches and network emission bright points at their bases. Very similar populations of dynamic features appear in the same loci of magnetic bushes with some changes.

Moreover, the present study illustrates some interesting aspects of MBP dynamic properties that have not previously been addressed in the literature. The most important result is that MBPs show very rapid variations synchronized with coronal line brightness. High Doppler velocities as well as strong magnetic field concentrations are very prominent in the chromospheric rosettes.

Sheeley & Golub (1979) reported that the collective coronal bright points are made up of substructures that control the behaviour of the chromospheric and coronal emission from these features.

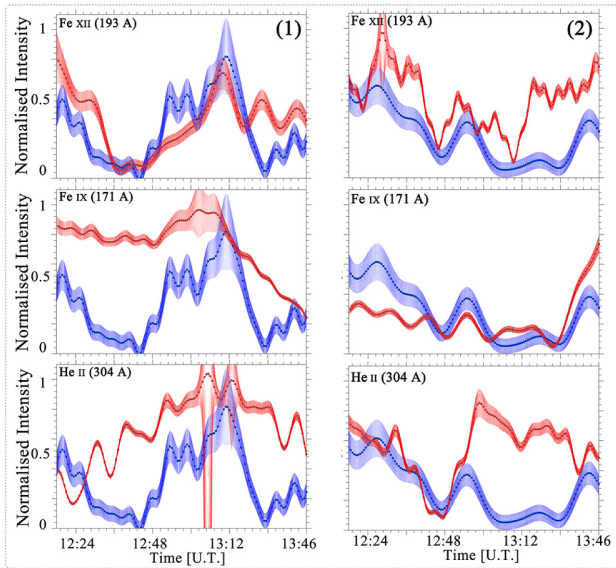


Figure 9. Time-intensity variations in the selected region (10×10 pixels²) marked as numbers 1 (left column) and 2 (right column) in Fig. 8. The blue squares show the *IRIS* Si iv intensity variation, and intensity flux in AIA channels shown in red.

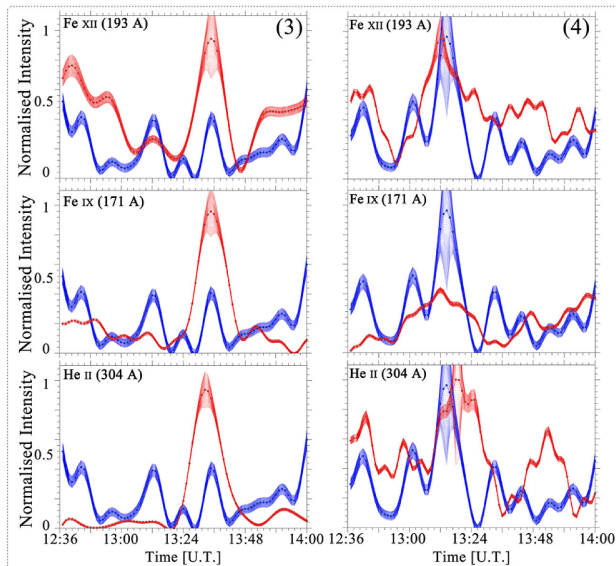


Figure 10. Time-intensity variation in the selected region (10×10 pixels²) marked as numbers 3 (left column) and 4 (right column) in Fig. 8. The blue squares show the *IRIS* Si iv intensity variation, and intensity flux in AIA channels shown in red.

Such rapid and simultaneous intensity fluctuations are confirmed in our findings. Prompt and synchronized intensity changes deducible from the radiative and conductive heating and cooling rates are intermittent in the upper solar atmosphere. If this is the case, it can be assumed that, as observed and reported, the energy supply from the TR into the corona could provide enough thermal energy to support the coronal EUV emissions.

Finally, the dopplergrams in cooler lines (C II and Mg II κ) demonstrate that a similar range of Doppler velocities in red is always associated with the same values of blue-shifted materials at nearby

locations. This could be attributed to miniature closed loops in the network regions in the lower layers of TR, whereas hotter Si iv dopplergrams are dominantly reddish in the magnetic network.

ACKNOWLEDGEMENTS

IRIS is a NASA small explorer mission developed and operated by LMSAL with mission operations executed at NASA ARC with the contribution of NSC (Norway). I am indebted to AIA/*SDO* for providing easy access to the calibrated data and the HMI/*SDO* team for the high-quality data supplied. I am also grateful to the Iran National Foundation INSF and extend my gratitude to Professor S. Koutchmy for useful discussions and his comments and remarks on this study. This work has also been partially supported by the Center for International Scientific Studies and Collaboration (CISSC). The AIA data are courtesy of *SDO* (NASA) and the AIA consortium and the French Institut d'Astrophysique de Paris-CNRS and UPMC. The comments and remarks from the anonymous referee were very helpful in improving the first version of this manuscript, and I wish to thank them for their detailed critical reading of this paper.

REFERENCES

- Alipour N., Safari H., 2015, *ApJ*, 807, 175
 De Pontieu B. et al., 2014, *Sol. Phys.*, 289, 2733
 Dunn R. B., Zirker J. B., 1973, *Sol. Phys.*, 33, 281
 Filippov B., Golub L., Koutchmy S., 2009, *Sol. Phys.*, 254, 259
 Golub L., Krieger A. S., Silk J. K., Timothy A. F., Vaiana G. S., 1974, *ApJ*, 189, L93
 Golub L., Krieger A. S., Vaiana G. S., 1975, *Sol. Phys.*, 42, 131
 Golub L., Krieger A. S., Harvey J. W., Vaiana G. S., 1977, *Sol. Phys.*, 53, 111
 Habbal S. R., Withbroe G. L., 1981, *Sol. Phys.*, 69, 77
 Hagenaar H. J., Schrijver C. J., Title A. M., 1997, *ApJ*, 481, 988
 Hart A. B., 1954, *MNRAS*, 114, 17
 Jafarzadeh S., Cameron R. H., Solanki S. K., Pietarila A., Feller A., Lagg A., Gandorfer A., 2014, *A&A*, 563, 101
 Kayshap P., Dwivedi B. N., 2017, *Sol. Phys.*, 292, 108
 Keller C. U., 1992, *Nature*, 359, 307
 Koutchmy S., Hara H., Suematsu Y., Reardon K., 1997, *A&A*, 320, L33
 Lawrence J. K., Schrijver C. J., 1993, *ApJ*, 411, 402
 Madjarska M. S., Doyle J. G., Teriaca L., Banerjee D., 2003, *A&A*, 398, 775
 Martinez-Sykora J. et al., 2015, *ApJ*, 803, 44
 Muller R., Dollfus A., Montagne M., Moity J., Vigneau J., 2000, *A&A*, 359, 373
 Pesnell W. D., Thompson B. J., Chamberlin P. C., 2012, *Sol. Phys.*, 275, 3
 Roudier T., Rieutord M., Brito D., Rincon F., Malherbe J. M., Meunier N., Berger T., Frank Z., 2009, *A&A*, 495, 945
 Sheeley N. R., Jr, Golub L., 1979, *Sol. Phys.*, 63, 119
 Sheeley N. R., Jr, Warren H. P., 2012, *ApJ*, 749, 40
 Simon G. W., Leighton R. B., 1964, *ApJ*, 140, 1120
 Snodgrass H. B., Ulrich R. K., 1990, *ApJ*, 351, 309
 Tavabi E., 2014, *Ap&SS*, 352, 43
 Tavabi E., Koutchmy S., Golub L., 2015, *Sol. Phys.*, 290, 2871
 Title A. M., Hoeksema J. T., Schrijver C. J., Aia Team, 2006, 36th COSPAR Scientific Assembly, CD ROM 2600
 Wang H., Zirin H., 1989, *Sol. Phys.*, 120, 1
 Zirin H., 1993, in Zirin H., Ai G., Wang H., eds, *IAU Colloq. 141, The Magnetic and Velocity Fields of Solar Active Regions*, Astronomy Society of the Pacific Conference Series Vol. 46, Astron. Soc. Pac., San Francisco, p. 215

This paper has been typeset from a $\text{\TeX}/\text{\LaTeX}$ file prepared by the author.